Aperture synthesis imaging of colored GEO objects

John Young[a], Christopher Haniff[a], David Buscher[a], Tanish Satoor[a], Matthew Le Maître[a], Michelle Creech-Eakman[b], and Ifan Payne[b]

[a]University of Cambridge, United Kingdom
[b]New Mexico Tech/Magdalena Ridge Observatory Interferometer, Socorro, United States

ABSTRACT

Interferometry provides the only practicable way to image satellites in Geosynchronous Earth Orbit (GEO) with sub-meter resolution. The Magdalena Ridge Observatory Interferometer (MROI) is being funded by the US Air Force Research Laboratory to deploy the central three unit telescopes in order to demonstrate the sensitivity and baseline-bootstrapping capability needed to observe GEO targets. In parallel, we are investigating the resolution and imaging fidelity that is achievable with larger numbers of telescopes. We present imaging simulations with 7- and 10- telescope deployments of the MROI, and characterize the impact of realistic spectral variations compared with a "gray" satellite.

Keywords: Image reconstruction, Optical interferometry, Satellite imaging

1. INTRODUCTION

Current ground-based filled-aperture telescopes do not provide a useful capability for imaging satellites in Geosynchronous Earth Orbit (GEO). The only practicable way to image GEO satellites with sub-meter resolution is to employ visible/infrared interferometry. The Magdalena Ridge Observatory Interferometer[1] (MROI) is being funded by the US Air Force Research Laboratory (AFRL) to determine the feasibility of imaging passively-illuminated GEO targets with a ground-based interferometer. A key part of this effort is to investigate the spatial resolution and imaging fidelity that can be achieved with different numbers of array elements, by means of computational simulations.

Our preliminary simulations[2] demonstrated that faithful reconstructions of a typical satellite can be obtained with 7 unit telescopes, and that increasing the number of telescopes to 10 improves the spatial resolution from 0.75 m to 0.5 m. Those results assumed simultaneous observations at a range of wavelengths in order to extend the Fourier plane coverage, since Earth rotation does not perform this function for GEO targets.

In reality, the effectiveness of this approach depends on the magnitude of the reflectivity variations between the various satellite components, and how these variations are accounted for in the image reconstruction process. In this paper we investigate the impact of realistic albedo variations with wavelength.

We also employ the same simulation framework to explore the image fidelity attainable for satellites approaching 30 m in overall extent, where the angular size of the target is large compared with the resolution of the MROI array and hence low spatial frequency measurements are not possible. This paper describes the simulation methods in Section 2, highlights the major results in Section 3, and finally summarizes our conclusions from the simulations carried out thus far (Section 4).

2. METHODS

We employed the same general methodology as in previous work.[2–4] There are two main steps in the simulation procedure: generating the interferometric data from a wavelength-dependent "truth image" of the observed object, and reconstructing these data to obtain a "gray" (i.e. wavelength-independent) estimate of the truth image.

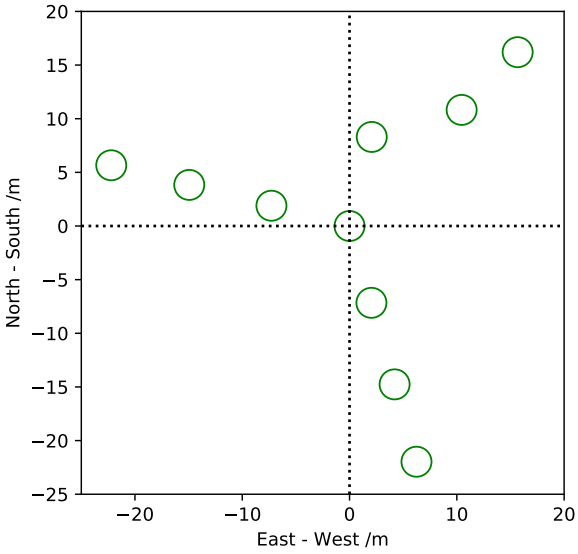

(a) MROI array configuration

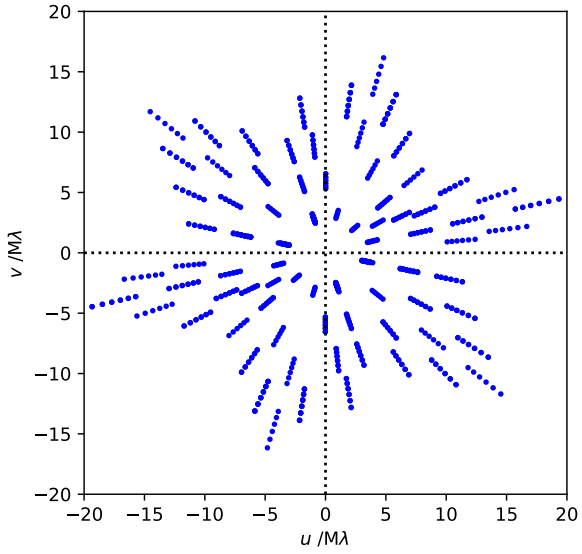

(b) MROI *uv* coverage

Figure 1. (a) The most compact Y-shaped array configuration, with all 10 MROI unit telescopes. The 7-telescope configuration is the same except that the outermost 3 telescopes are removed. (b) The corresponding *uv*-plane coverage assuming 10 unit telescopes and five 90 nm wide spectral channels from 1960 nm to 2410 nm.

2.1 General procedure

A model of a GEO target was adopted, and synthetic data generated as though the target had been observed with a ground-based 7- or 10-element near-IR interferometer and, optionally, a single dish telescope. These data were then used as input to the image reconstruction code `BSMEM`[*5] and the resulting reconstructed images were evaluated.

We used an in-house data simulation program called `vsim` to generate an OIFITS[6] file containing noisy power spectrum and bispectrum data as though the target had been observed using either a 7- or 10-telescope realisation of the MROI. The target was assumed to be in an equatorial orbit and at the observational meridian during the observations.

Fourier data were generated for five spectral channels within the 2.2 µm K band. Each channel had a bandwidth of 90 nm and these were centred at wavelengths of 2005 nm, 2095 nm, 2185 nm, 2275 nm and 2365 nm. The resulting *uv* coverage and the layout of the telescopes on the ground are shown in Fig. 1. The simulation code allowed a different truth image to be specified for each wavelength channel, in order to simulate a non-gray target.

We assumed K-band magnitudes in the range 8–11 for our targets. The 10^{th} and 11^{th} magnitude targets were representative of typical geosynchronous satellites.[7] We assumed excellent seeing conditions for the MROI site of 0.7″. To optimize the overall signal-to-noise of the imaging fringe measurements, we expect to interfere sub-arrays of the available unit telescopes. We simulated five consecutive snapshots, each combining six telescopes, in order to generate all of the Fourier data accessible with a 10-element array (or two snapshots for a 7-element array). An incoherent exposure time of 100 s per "snapshot" was assumed. Assuming 20 s to reconfigure the optics feeding the beam combiner prior to each snapshot, we estimate the total time to observe a satellite and nearby calibrator star at 1200 s.

Random errors were added to the synthetic Fourier data, to mimic the effects of photon noise, detector readout noise, and calibration errors as realistically as possible. The calibration errors were assumed to be 2% for the power spectra and 0.8° for the bispectrum phases.

Images were reconstructed from the simulated MROI observations using `BSMEM`, which finds the image with the highest entropy (i.e. the least information) that is consistent with the data. An important feature of `BSMEM` is the automatic estimation of the hyper-parameter α that controls the weighting of the entropic prior relative to the likelihood. The only mandatory user inputs are the interferometric data and a prior image that is used as a reference when calculating the entropy. In its

*http://www.mrao.cam.ac.uk/research/optical-interferometry/bsmem-software/

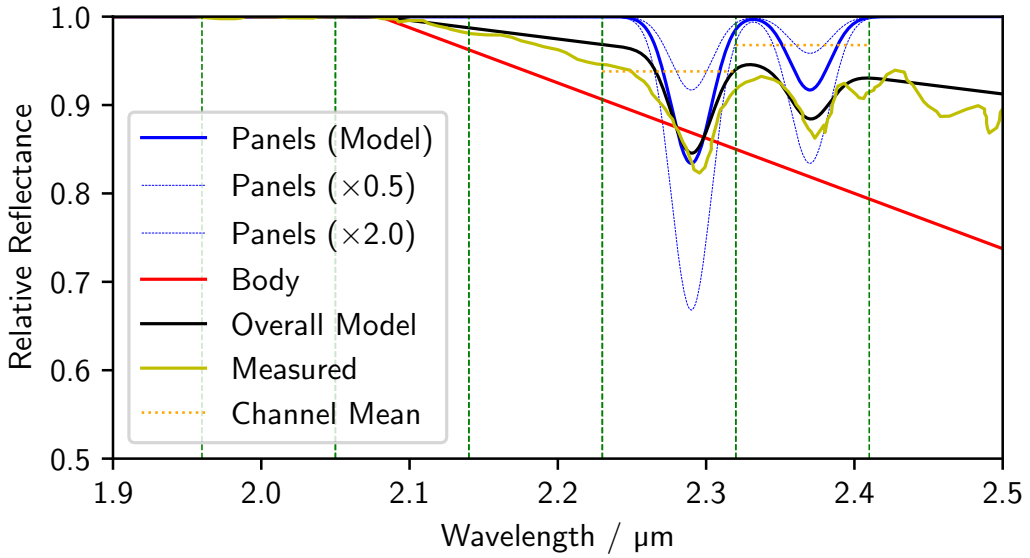

Figure 2. The albedo model used for the simulated Meteor satellite based on reflectance spectra from a Palapa-B GEO target.[8] The recorded data and model are shown for both the bus and the solar array, as well as the recorded spectra. Drawn in blue are the model for the panels that fits the recorded spectrum (heavy line), and the same model multiplied by 0.5 and 2.0 respectively, as used to explore the effect of different levels of albedo variation. The dashed vertical lines delineate the 90 nm-wide MROI spectral channels.

standard mode of operation, the program stops automatically when the reduced χ^2 between the reconstructed image and the data reaches unity.

For previous satellite reconstructions, we employed a two-step reconstruction procedure for running `BSMEM`.[3] For this work the procedure was generalized to a N-step one. An initial reconstruction was made using only short baseline data, corresponding to low spatial frequency structures such as the satellite's solar panels, and an uninformative circular Gaussian prior image. At each subsequent iteration, additional high spatial frequency data from the full dataset were added, and an image derived from the previous iteration was used as the prior image. To derive the intermediate prior images, each intermediate result was blurred by convolving with a Gaussian, then pixels below a pre-defined threshold were set to zero in order to remove reconstruction artefacts. A total of either two or ten iterations were used. In most cases, the two- and ten-iteration reconstructions are very similar.

2.2 Satellite models

In the first instance AFRL supplied us with a TASAT image of a Meteor-1 class Low Earth Orbit (LEO) satellite (Fig. 3a). This class of satellite has a bus that is roughly 1.5×1.5×5 meters in size, together with solar panels that extend approximately 6 m on each side. Scaled versions of this image were used to mimic GEO satellites of different sizes.

In order to assess the impact of variations in albedo with wavelength on the imaging results, two alternative satellite models were created. A FITS image cube was created from the 2D Meteor-1 image, using an ad-hoc spectral model based on passive reflectance data from a Palapa-B satellite in GEO.[8] The model, illustrated in Fig. 2, assumes that the albedo of the bus varies linearly with wavelength, and that the albedo of the solar panels is constant except for Gaussian absorption peaks at 2290 nm and 2370 nm, whose depths were scaled to fit the measured spectra.

The second non-gray alternative was an image cube of DirecTV-9S (Fig. 3b), a large (29 m span) communications satellite. The wavelength variations for DirecTV-9S were calculated using the TASAT software by AFRL staff. TASAT simulates the reflectance properties of the constituent materials and hence is capable of very accurate results.[9] The properties of some materials used in DirectTV-9S were not known, hence similar materials used in other satellites were assumed.

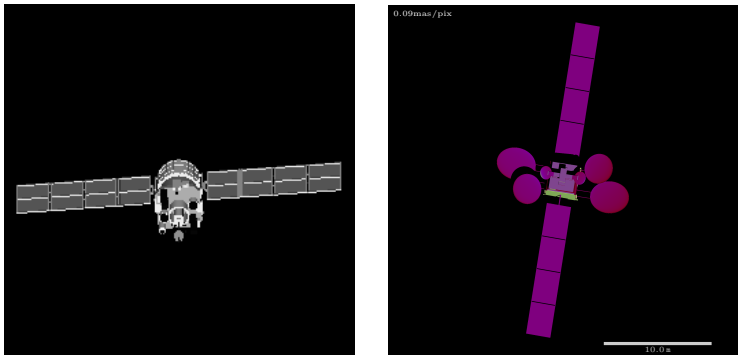

(a) Meteor-1 truth image (b) DirecTV-9S truth image

Figure 3. (a) The Meteor-1 satellite truth image used as the basis for our ad-hoc chromatic model. (b) The 1960 nm–2050 nm layer of the DirecTV-9S TASAT truth image, using a color map to display the gray levels.

3. RESULTS

3.1 Imaging small satellites

The relationship between reconstruction fidelity and satellite extent was investigated, firstly using the gray Meteor model, then using the two wavelength-dependent models. The Meteor images were scaled to a number of sizes, ranging from 1.6 m to 15.6 m. Dimensions up to 29.0 m were considered for DirecTV. To ensure that the image fidelity was not limited by poor signal-to-noise, we initially assumed the targets to be 8^{th} magnitude for this investigation, before extending the simulations to fainter satellites.

For image reconstruction from the wavelength-dependent models, the hyper-parameter α was set manually to match the value determined automatically by `BSMEM` for the gray satellite. This was necessary to prevent over-fitting and ensure convergence, as `BSMEM` would otherwise have attempted to find a "gray" image giving unit reduced χ^2 over the measured spectral visibilities. Fixing the regularization level permitted a degree of mis-fitting, hopefully representative of the channel-to-channel varations in the satellite appearance. If the observations were of a real satellite, an empirical approach such as the "L-curve" method[10] could have been used to find the optimum regularization level.

Sample imaging results for the wavelength-dependent Meteor satellite model are shown in Fig. 4. These exhibit a spatial resolution of ~0.7 m for the 7-telescope images and ~0.5 m for the 10-telescope images, more or less independently of the satellite size. It was found that satellites as small as 2.6 m could reliably be recovered using the most compact MROI configuration at K band. The interferometer resolution could be better matched to smaller satellites by using shorter observing wavelengths, and/or a more extended array configuration. In practice, the limiting factor for observing small satellites (smaller than a few meters) will be the difficulty of acquiring and tracking fringes on such faint targets. 10-telescope reconstructions for DirecTV at more realistic magnitudes $m_K = 10$ and $m_K = 11$ and sizes up to 29 m are shown in Fig. 5. These illustrate that the spatial resolution achieved is largely independent of the target brightness, as expected.

3.2 Extreme albedo variation with wavelength

The effect of increasingly extreme albedo variation with wavelength was investigated using a derivative of the 3D Meteor model. The albedo of the satellite bus was left unchanged, but the Gaussian absorption peaks of the solar panels were multiplied by a linear factor k_{pk}. Figure 2 shows the original model as well as the modified model for k_{pk} values of 0.5 and 2.0. For reconstructions with 7 telescopes, convergence became unreliable for $k_{\text{pk}} > 12.6$ (corresponding to an average reflectance of 22% in channel 4 and 59% in channel 5), whereas reconstructions with 10 telescopes failed to converge reliably for $k_{\text{pk}} > 10.3$. In both cases, the detrimental effect on image fidelity was fairly slight for panel absorption features exaggerated by factors up to 10.

Extreme albedo variations were also simulated using the DirecTV-9S TASAT images. The TASAT outputs reflect the true satellite albedo, which is close to that of the original 3D Meteor model. The albedo of the solar array in the fourth spectral channel was scaled by a factor k_{ch}, and the fifth channel such that the ratio of the absorption peak heights remained constant. The pixels corresponding to the solar panels were selected using a mask. Example results are presented in Fig. 6.

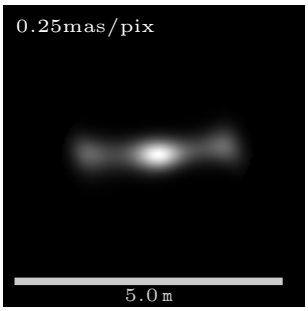

(a) 3.1 m, 10-Tel.

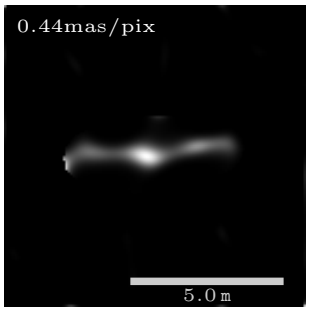

(b) 5.5 m, 10-Tel.

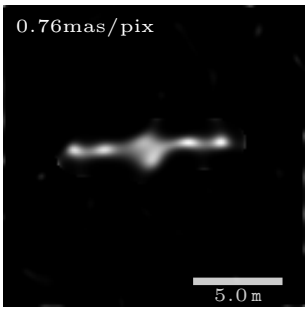

(c) 9.4 m, 10-Tel.

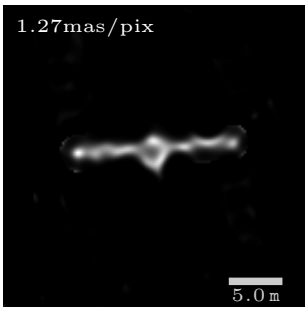

(d) 15.6 m, 10-Tel.

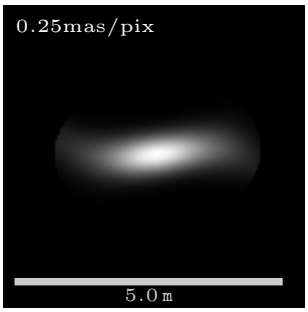

(e) 3.1 m, 7-Tel.

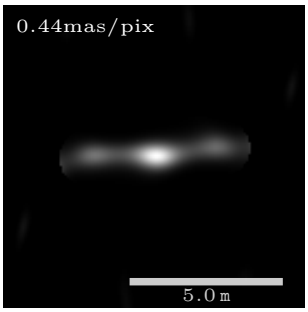

(f) 5.5 m, 7-Tel.

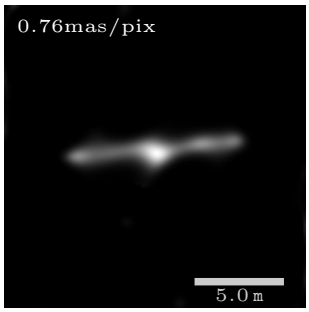

(g) 9.4 m, 7-Tel.

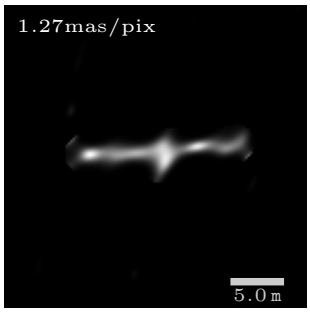

(h) 15.6 m, 7-Tel.

Figure 4. Reconstruction examples using 7 and 10 telescopes for a range of 3D Meteor target sizes (maximum extent given below each image) at 8^{th} magnitude. The appearance of an oscillating intensity across the panels is visible in the 10-telescope data, whilst the 7-telescope images remain relatively uniform. This is likely due to partial resolution of the panel sub-structure.

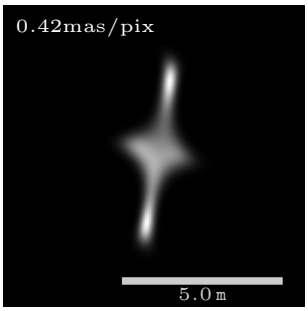

(a) 5.8 m, $m_K = 10$

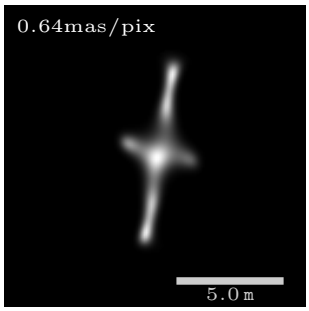

(b) 8.7 m, $m_K = 10$

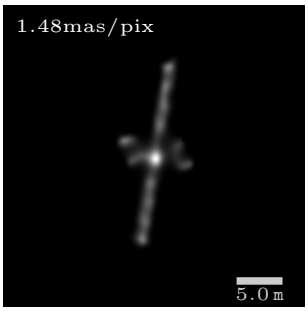

(c) 20.3 m, $m_K = 10$

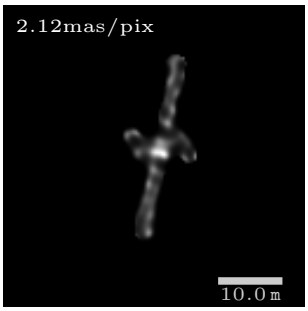

(d) 29.0 m, $m_K = 10$

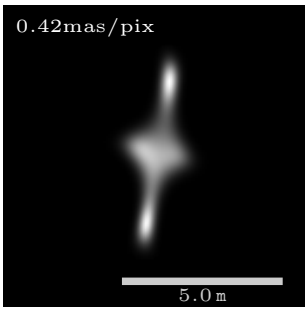

(e) 5.8 m, $m_K = 11$

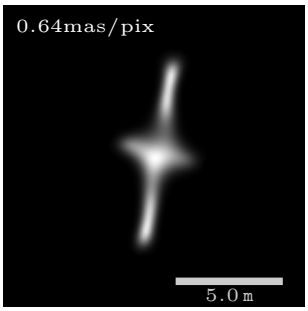

(f) 8.7 m, $m_K = 11$

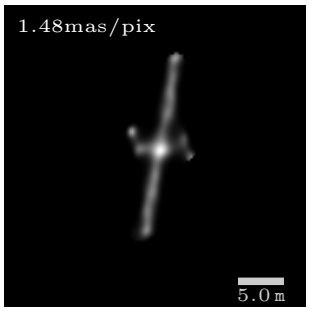

(g) 20.3 m, $m_K = 11$

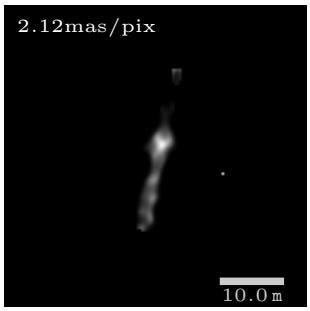

(h) 29.0 m, $m_K = 11$

Figure 5. 10-telescope reconstructions of the DirecTV-9S model at 10^{th} and 11^{th} magnitude for a range of satellite sizes. The maximum extent of the satellite is shown beneath each image.

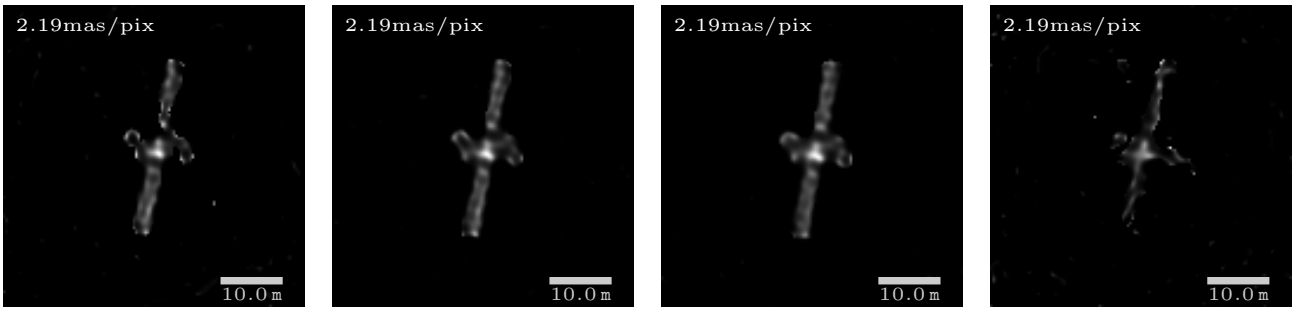

(a) 10 Tel., k_{ch} = 1.6 (b) 10 Tel., k_{ch} = 1.2 (c) 10 Tel., k_{ch} = 0.9 (d) 10 Tel., k_{ch} = 0.4

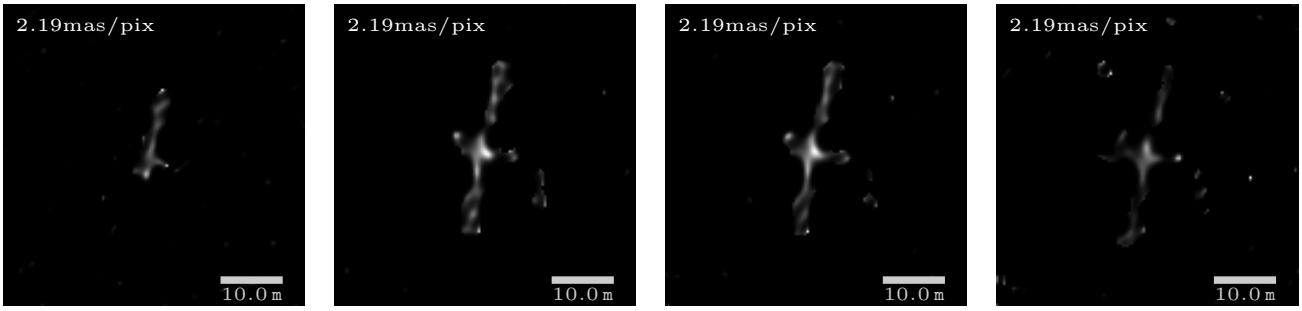

(e) 7 Tel., k_{ch} = 1.6 (f) 7 Tel., k_{ch} = 1.2 (g) 7 Tel., k_{ch} = 0.9 (h) 7 Tel., k_{ch} = 0.4

Figure 6. A selection of reconstructions of the 29.0 m DirecTV-9S satellite at 8th magnitude with the albedo over MROI spectral channel 4 scaled by k_{ch}, and channel 5 scaled appropriately based on the Meteor model. Note that decreasing k_{ch} is more damaging to fidelity than increasing k_{ch}.

BSMEM converged for $0.5 < k_{ch} \lesssim 1.9$, and the main features of the satellite were identifiable for $0.75 \geq k_{ch} \lesssim 1.5$. The results from both models demonstrate conclusively that even extreme albedo variations between spectral channels will not be a barrier to successful image reconstruction.

3.3 Imaging large satellites: fusion with short-baseline data

Large targets can be problematic because the minimum MROI baseline is limited by the size of the unit telescope enclosures to 7.8 m, corresponding to 10.2 m spatial resolution for a GEO target observed at 2.2 µm wavelength. This can be addressed by using contemporaneous observations with a large single telescope to sample low spatial frequencies. We have assumed that the single telescope observations use the Non-Redundant Masking (NRM) technique, effectively turning the telescope into an interferometer. The Magdalena Ridge Observatory hosts a 2.4 m telescope, which could be used for NRM observations of GEO targets.

We simulated masked observations with either a 4.0 m or 2.4 m telescope. The aperture mask and corresponding uv coverage are drawn in Fig. 7. The noise model adopted for the NRM data assumed the use of a 100×100 pixel detector region to sample the two-dimensional fringe pattern and detector readout noise of 0.2 e^-. We conservatively assumed calibration errors of 5% for the power spectra and 2° for the bispectrum phases, significantly worse than the MROI values (2% and 0.8°). The calibration errors dominated the photon and detector readout noise, hence the final SNR was similar for the 4.0 m and 2.4 m telescopes despite the difference in sub-aperture sizes. We simulated simultaneous MROI and NRM observations of the DirecTV satellite model at sizes of 15.0 m and 30.0 m, and merged the OIFITS datasets for reconstruction with BSMEM.

Reconstructed images are presented in Fig. 8. These clearly show that the NRM data was of negligible value for the 15.0 m satellite, but was required for successful recovery of the 30.0 m satellite. The 4.0 m NRM data offered no significant advantage over the 2.4 m NRM.

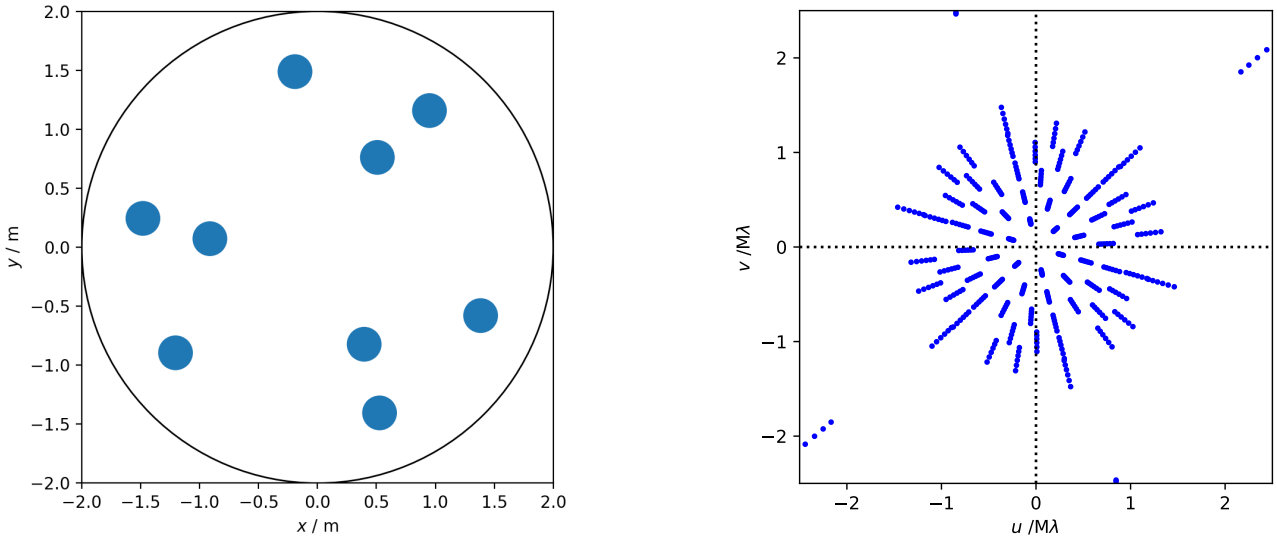

(a) NRM mask

(b) NRM *uv* coverage

Figure 7. (a) The position of the sub-apertures in the 4.0 m mask. Each sub-aperture is 0.59 m in diameter (the 2.4 m mask is a scaled version of this, using 0.35 m sub-apertures). (b) The corresponding *uv* coverage, with some of the inner MROI coverage visible towards the edges.

4. CONCLUSIONS

We have used computational simulations to investigate two factors that could potentially limit MROI's capability to image GEO satellites. Realistic albedo variations between spectral channels within the 2.2 µm K-band were found to have a negligible effect on the reconstructed images, for a range of satellite sizes and for satellites as faint as $m_K = 11$. Useful images were obtained even with exaggerated albedo variations.

The combination of aperture masking data with the MROI data was found to be beneficial for large satellites (~30 m). There was no significant advantage to using a 4.0 m masked telescope rather than a 2.4 m one.

We plan further simulations to quantify the impact of time-varying solar illumination on the reconstructed images, using TASAT images that have already been generated.

Disclaimer The views and conclusions contained herein are those of the authors and should not be interpreted as necessarily representing the official policies or endorsements, either expressed or implied, of Air Force Research Laboratory (AFRL) and or the U.S. Government.

ACKNOWLEDGMENTS

This material is based on research sponsored by Air Force Research Laboratory (AFRL) under agreement number FA9453-15-2-0086. The U.S. Government is authorized to reproduce and distribute reprints for Governmental purposes notwithstanding any copyright notation thereon. We thank Brandon Mueller for generating the TASAT images.

REFERENCES

[1] Buscher, D. F., Creech-Eakman, M., Farris, A., Haniff, C. A., and Young, J. S., "The Conceptual Design of the Magdalena Ridge Observatory Interferometer," *Journal of Astronomical Instrumentation* **2**, 1340001 (2013).

[2] Young, J., Haniff, C., Buscher, D., Creech-Eakman, M., and Payne, I., "High fidelity imaging of geosynchronous satellites with the MROI," in [*Optical and Infrared Interferometry and Imaging V*], *Proc. SPIE* **9907**, 99073I (2016).

[3] Young, J., Haniff, C., Buscher, D., Creech-Eakman, M., Payne, I., Jurgenson, C., and Romero, V., "The MROI's capabilities for imaging geosynchronous satellites," in [*Optical and Infrared Interferometry III*], *Proc. SPIE* **8445**, 84452N (2012).

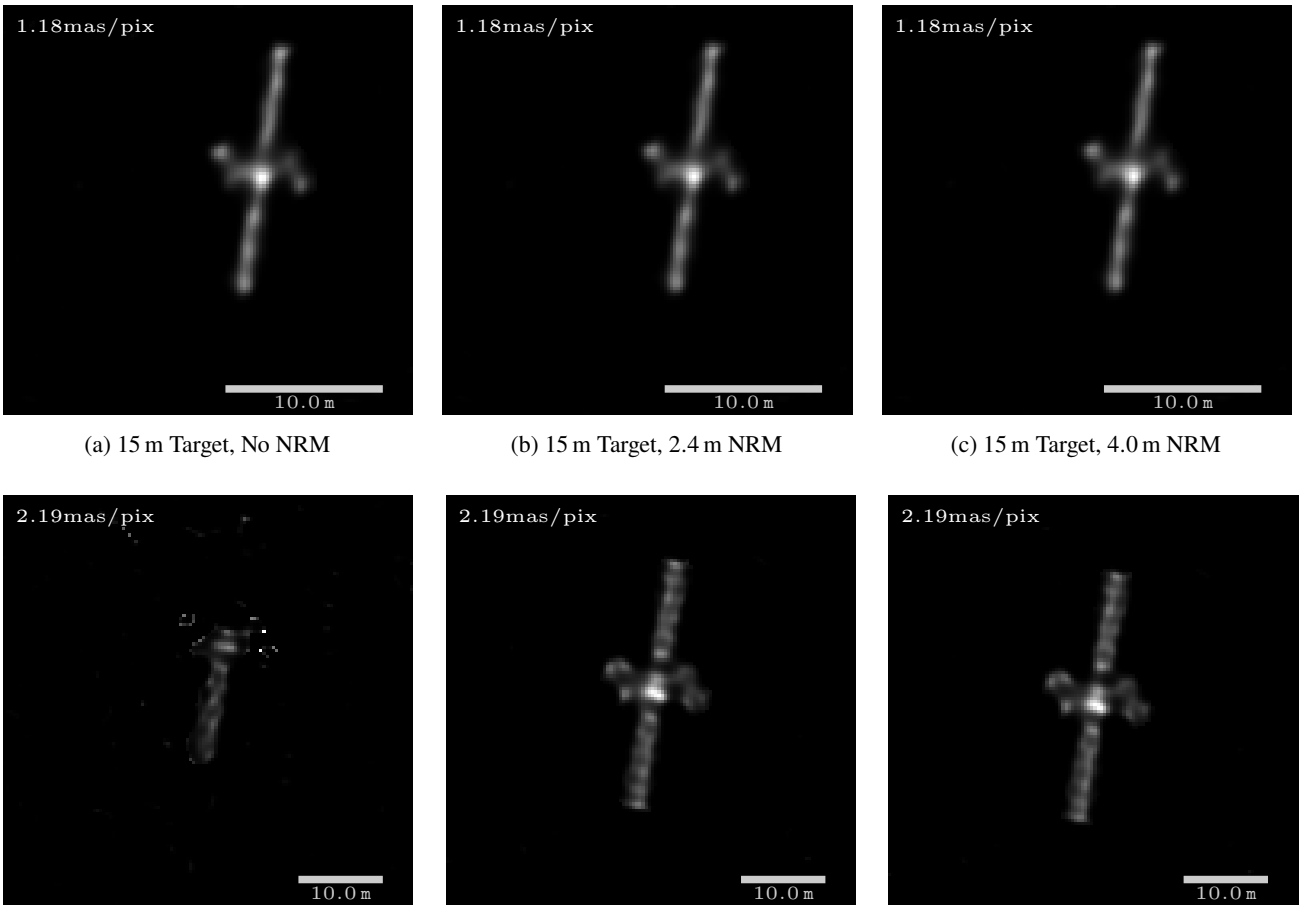

(a) 15 m Target, No NRM (b) 15 m Target, 2.4 m NRM (c) 15 m Target, 4.0 m NRM

(d) 30 m Target, No NRM (e) 30 m Target, 2.4 m NRM (f) 30 m Target, 4.0 m NRM

Figure 8. The reconstructions of the 15.0 m and 30.0 m satellites using 10-telescope MROI data with either 2.4 m NRM data, 4.0 m NRM data, or no NRM data. The fidelity increase was most prominent for the largest satellite, as expected. Both NRM sizes produced comparable reconstructions. The position of the object within the image is not significant, as squared visibilities and bispectra are invariant to translation of the source.

[4] Young, J., Haniff, C., and Buscher, D., "Interferometric imaging of geo-synchronous satellites with ground-based telescopes," in [*2013 IEEE Aerospace Conference*], (2013).

[5] Buscher, D. F., "Direct maximum-entropy image reconstruction from the bispectrum," in [*Very High Angular Resolution Imaging*], *IAU Symposium Series* **158**, 91 (1994).

[6] Pauls, T. A., Young, J. S., Cotton, W. D., and Monnier, J. D., "A Data Exchange Standard for Optical (Visible/IR) Interferometry," *Publications of the Astronomical Society of the Pacific* **117**, 1255 (2005).

[7] Sanchez, D. J., Gregory, S. A., Werling, D., Payne, T. E., Kann, L., Finkner, L. G., Payne, D. M., and Davis, C. K., "Photometric measurements of deep space satellites," in [*Imaging Technology and Telescopes*], *Proc. SPIE* **4091**, 164 (2000).

[8] Abercromby, K. J., Buckalew, B., Abell, P., and Cowardin, H., "Infrared Telescope Facility's Spectrograph Observations of Human-Made Space Objects," in [*Advanced Maui Optical and Space Surveillance Technologies Conference (AMOS)*], *NASA Technical Reports*, JSC–CN–33037 (2015).

[9] Riker, J. F., Crockett, G. A., and Brunson, R. L., "Time-domain analysis simulation for advanced tracking," in [*Acquisition, Tracking, and Pointing VI*], *Proc. SPIE* **1697**, 297 (1992).

[10] Hansen, P., "Analysis of Discrete Ill-Posed Problems by Means of the L-Curve," *SIAM Review* **34**(4), 561 (1992).